Modification of the Thomas model for predicting unsymmetrical breakthrough curves using an adaptive neural-based fuzzy inference system

Mohammad Javad Amiri, Maryam Khozaei and Antonio Gil

ABSTRACT

The Thomas equation is a popular model that has been widely used to predict breakthrough curves (BTCs) when describing the dynamic adsorption of different pollutants in a fixed-bed column system. However, BTCs commonly exhibit unsymmetrical patterns that cannot be predicted using empirical equations such as the Thomas model. Fortunately, adaptive neural-based fuzzy inference systems (ANFISs) can be used to model complex patterns found in adsorption processes in a fixed-bed column system. Consequently, a new hybrid model merging Thomas and an ANFIS was introduced to estimate the performance of BTCs, which were obtained for Cd(II) ion adsorption on ostrich bone ash-supported nanoscale zero-valent iron (nZVI). The results obtained showed that the fair performance of the Thomas model ($NRMSE = 27.6\%$ and $E_f = 64.6\%$) improved to excellent ($NRMSE = 3.8\%$ and $E_f = 93.8\%$) due to the unique strength of ANFISs in nonlinear modeling. The sensitivity analysis indicated that the initial solution pH was a more significant input variable influencing the hybrid model than the other operational factors. This approach proves the potential of this hybrid method to predict BTCs for the dynamic adsorption of Cd(II) ions by ostrich bone ash-supported nZVI particles.

Key words | adsorption process, ANFIS, nanoscale zero-valent iron, ostrich bone ash, Thomas model

Mohammad Javad Amiri (corresponding author)
Department of Water Engineering, College of Agriculture,
Fasa University,
74617-81189 Fasa,
Iran
E-mail: mj_amiri@fasau.ac.ir

Maryam Khozaei
Department of Water Engineering, College of Agriculture,
Shiraz University,
Shiraz 71365,
Iran

Antonio Gil
Department of Sciences,
Public University of Navarra, Campus of Arrosadia,
31006 Pamplona,
Spain

INTRODUCTION

Cadmium compounds are extensively applied in many industries such as metal plating facilities, paint pigments, mining operations, stabilizers and silver-cadmium batteries (Boparai *et al.* 2011). The release of these compounds into the environment can cause adverse health effects for humans such as kidneys disease, high blood pressure, lung insufficiency and bone defects (Boparai *et al.* 2011). As a result, cadmium is considered as priority pollutant by the Agency for Toxic Substances and Disease Registry of the USA (www.atsdr.cdc.gov). The maximum concentration level of cadmium in drinking water is 0.005 mg L^{-1} as set by the Council of the European Communities in 1976.

Adsorption has been considered to be an alternative method to conventional and modern wastewater treatments for the removal of Cd(II) from wastewater due to its high efficiency, simplicity, low-cost and adaptability (Boparai *et al.* 2011; Boparai *et al.* 2013). A great deal of attention has recently focused on the application of nanoscale zero-valent iron (nZVI) for the elimination of heavy metals (Zhang *et al.* 2011; Soleymanzadeh *et al.* 2015; Gil *et al.* 2018). However, nZVI has limited applications in waste-water treatment due to its tendency to aggregate and oxidize (Zhang *et al.* 2011; Gil *et al.* 2018). To resolve this problem, porous materials such as ostrich bone ash has been employed to support nZVI (Arshadi *et al.* 2015; Gil

et al. 2018), which can subsequently be separated using an external magnetic field without the need for filtration and centrifugation. Although several researchers (Boparai *et al.* 2011; Boparai *et al.* 2013; Zhang *et al.* 2014; Soleymanzadeh *et al.* 2015) have shown the potential of stabilized nZVI as an adsorbent for Cd(II) removal under laboratory batch conditions, the performance of nZVI supported on porous materials for Cd(II) ion removal in a fixed-bed column has not been investigated.

The performance of fixed-bed adsorption is assessed by plotting an effluent concentration-time profile or breakthrough curve (BTC). However, as fixed-bed adsorption experiments are costly, difficult and time-consuming, an ability to predict BTCs could be a good and speedy alternative to the measurable column experiments for describing the adsorption process in fixed-bed systems. Therefore, a variety of mathematical empirical equations such as Bohart–Adams (Bohart & Adams 1920), Thomas (Thomas 1944), bed-depth service time (BDST) (Hutchins 1973) and Yoon–Nelson (Yoon & Nelson 1984) have been widely used to describe BTCs. Of these, the Thomas model is the most widely used due to its simplicity and applicability for different pollutants. This model is appropriate to predict the adsorption process when internal and external diffusion resistances can be ignored. Furthermore, this model supposes that the adsorption process is described by pseudo-second-order reversible reaction kinetics and Langmuir isotherm at equilibrium (Han *et al.* 2007; Hasan *et al.* 2010; Chowdhury & Saha 2013). This model considered that the adsorption process is not limited by the chemical reaction but controlled by the mass transfer at the interface (Hasan *et al.* 2010; Chowdhury & Saha 2013). Although these traditional methods, particularly the Thomas model, are able to well predict symmetrical BTCs, they are not particularly suitable for data fitting with unsymmetrical BTCs (Tovar-Gomez *et al.* 2013).

In recent years, artificial neural networks (ANNs) have been successfully used to estimate the performance of BTCs (Cavas *et al.* 2011; Chowdhury & Saha 2013; Tovar-Gomez *et al.* 2013; Oguz & Ersoy 2014; Masomi *et al.* 2015; Oguz 2017). To date, no studies have considered the adaptive neural-based fuzzy inference system (ANFIS) even though this model can be employed as an alternative when modeling complex input–output dependencies, like estimation of the elastic constant of rocks (Singh *et al.* 2012), evapotranspiration

estimation (Kisi & Ozturk 2007), prediction of nitrate (Mousavi & Amiri 2012), predicting lead removal from aqueous media (Amiri *et al.* 2013), leaf area prediction (Amiri & Shabani 2017), etc. The ANFIS can model the complex patterns seen in adsorption processes in a fixed-bed column system. In the present work, a new hybrid approach that combines both the Thomas and ANFIS models to estimate the performance of BTCs for the adsorption of Cd(II) ions by ostrich bone ash-supported nZVI is presented. The normalized root mean square error (*NRMSE*), efficiency (E_f) and linear regression were calculated for both observed and estimated data in order to evaluate the performance of this hybrid approach.

MATERIALS AND METHODS

Materials

Chemicals purchased from Aldrich Co. (Germany), including $Cd(NO_3)_2$ $4H_2O$, $FeCl_2$ $4H_2O$, $NaBH_4$, HCl and NaOH, were of analytical grade. Different concentrations of cadmium(II) were prepared by diluting a stock solution ($1,000$ mg L^{-1}).

Preparation of the adsorbent

The ostrich bone waste used in these experiments was obtained from a local butcher's store. The following procedure was used to prepare ostrich bone ash (OBA):

$$\text{Ostrich bone waste} \xrightarrow[\text{Dried at } 70^\circ\text{C for } 24\,\text{h}]{\text{Boiling in water}/2\,\text{h}}$$

$$\text{Solid wastes} \xrightarrow[\text{Pulverized with a } 45-80 \text{ range mesh}]{\text{Burning in air at } 550^\circ\text{C for } 24\,\text{h}} \text{OBA}$$

Ostrich bone ash-supported nZVI was prepared by reducing $FeCl_3.6H_2O$ using $NaBH_4$ as a reducing agent and ostrich bone ash as a support material, following the procedure reported by Zhang *et al.* (2011). Briefly, 10 g of $FeCl_3.6H_2O$ and 4 g of ostrich bone ash were mixed in 100 mL of ethanol/water mixture (30%, v/v) and shaken for 30 min at room temperature. A sodium borohydride solution containing 1.8 g of $NaBH_4$ in 100 mL deionized water was then added dropwise while stirring under an N_2 atmosphere. The resulting black particles were allowed to settle

and filtered using a vacuum filtration funnel. The average pore diameter and pore volume of the adsorbent obtained, which displayed a mesoporous structure, were 11 nm and $0.31\ cm^3\ g^{-1}$, respectively. The specific surface area was $108.9\ m^2\ g^{-1}$, thus indicating the high adsorption capacity for Cd(II) ions. Ca, P and Fe were found to be present in 24.2, 14.1 and 18.9 wt.%, respectively, thus showing the successful stabilization of nZVI. This adsorbent is fully characterized in the supplementary data (available with the online version of this paper) and explained by detail in a previous study from our group (Amiri *et al.* 2017).

Column experiments

Continuous flow experiments were conducted in a glass column with an i.d. of 2 cm and a height of 25 cm. A schematic diagram of the laboratory column study is presented in Figure S5 (available online). Cadmium(II) solution was fed upward into the columns using a peristaltic pump to maintain a constant flow rate. Cadmium(II) BTC was determined using different influent concentrations (50, 100 and 150 mg L^{-1}), bed heights (8, 12 and 16 cm), feed flow rates (0.5, 1, 1.5, 10, 20 and 30 mL min^{-1}) and pH (2, 5, 7 and 9). The effluent samples were collected at pre-defined time intervals and the Cd(II) concentration determined using atomic absorption spectroscopy. The following equations were employed to investigate the column data (Cavas *et al.* 2011):

$$\text{Effluent volume} = Q * t_e \tag{1}$$

Total amount of metal ions sent through the column
$$(m_{total},\ mg) = \frac{C_O * Q * t_e}{1000} \tag{2}$$

Total quantity of metal ions adsorbed in the column
$$(m_{ads},\ mg) = Q * \int_{t=0}^{t=t_e} C_{ad}\ dt \tag{3}$$

$$\text{Removal percentage} = \frac{m_{ads}}{m_{total}} * 100 \tag{4}$$

$$q_{ads} = \frac{m_{ads}}{M} \tag{5}$$

where C_o, C_e and C_{ad} are inlet, outlet and adsorbed metal ion concentrations, respectively, Q is the flow rate (mL min^{-1}), t_e is the bed exhaustion time (min), and M is the mass of the adsorbent in the column.

Modeling approach

The ANFIS model used was a five-layer ANN-FIS system. Further details of the five-layer ANFIS architecture are presented in the supplementary data. The ANFIS structure with two inputs, two rules based on Sugeno fuzzy rules and one output are presented in Figure S6 (available online) (Singh *et al.* 2012). Determination of the number and type of membership functions for input parameters, and definition of the type of membership functions for output data, are the most important steps for modeling by ANFIS. In this regard, the optimal ANFIS construction was selected using trial and error. Of the eight membership functions (i.e. trimf, dsigmf, psigmf, gbellmf, pimf, trapmf, gaussmf and gauss2mf) Gaussian has the best performance in terms of the mean square error (*MSE*) due to its smoothness, concise notation and non-zero at each point. Furthermore, a hybrid algorithm combining gradient descent and least-squares method was employed when learning the model. The complexity of the ANFIS model is determined using the number of membership functions for each input value. The results showed that the error was not significantly changed when the membership function was increased from three to four. Thus, three membership functions were selected for each input value for the rest of the modeling. Finally, the linear membership functions were chosen for the output parameters to increase the model accuracy. The performance of the ANFIS model should be controlled using an individual dataset as this model is based on trial and error. In this regard, the experimental data gathered from dynamic adsorption of Cd(II) in a packed bed column were divided into two groups: 200 of the available data points (70% of the observations) were randomly selected for training and the remaining 85 (30% of the observations) were used for testing. A hybrid model combining ANFIS and the Thomas equation was employed in MATLAB software Version 8.1. In this hybrid model, four operational parameters including inflow rate (Q), initial Cd(II) concentration (C_o), bed height (H), and initial solution pH, were taken as input data for the ANFIS model and the q_{ads} and k_{Th} for the Thomas equation was taken as output (see Figure 1). Subsequently, q_{ads} and k_{Th} which were calculated initially, were used as input data the for Thomas equation and $\frac{C_t}{C_o}$ was calculated as the final output. The flowchart of computations in the ANFIS–Thomas model is presented in Figure 2.

Evaluation criteria

The performance of the hybrid model for predicting BTC was evaluated using different statistical criteria including the determination coefficient (R^2), efficiency (E_f) and NRMSE.

$$R^2 = \frac{\sum_{i=1}^{n}\left[\left[\left(\frac{C_t}{C_o}\right)_{pre} - \left(\frac{\overline{C_t}}{C_o}\right)_{pre}\right]\left[\left(\frac{C_t}{C_o}\right)_{mea} - \left(\frac{C_t}{C_o}\right)_{mea}\right]\right]}{\sum_{i=1}^{n}\left[\left(\frac{C_t}{C_o}\right)_{mea} - \left(\frac{\overline{C_t}}{C_o}\right)_{mea}\right]^2 \sum_{i=1}^{n}\left[\left(\frac{C_t}{C_o}\right)_{pre} - \left(\frac{\overline{C_t}}{C_o}\right)_{pre}\right]^2} \tag{6}$$

$$E_f = \frac{\sum_{i=1}^{n}\left[\left(\frac{C_t}{C_o}\right)_{mea} - \left(\frac{\overline{C_t}}{C_o}\right)_{mea}\right]^2 - \sum_{i=1}^{n}\left[\left(\frac{C_t}{C_o}\right)_{mea} - \left(\frac{C_t}{C_o}\right)_{pre}\right]^2}{\sum_{i=1}^{n}\left[\left(\frac{C_t}{C_o}\right)_{mea} - \left(\frac{\overline{C_t}}{C_o}\right)_{mea}\right]^2}$$
$$*100 \tag{7}$$

$$NRMSE = \left[\frac{\sum_{i=1}^{n}\left[\left(\frac{C_t}{C_o}\right)_{pre} - \left(\frac{C_t}{C_o}\right)_{mea}\right]^2}{n\left[\left(\frac{\overline{C_t}}{C_o}\right)_{mea}\right]^2}\right]^{0.5} *100 \tag{8}$$

where $\left(\frac{C_t}{C_o}\right)_{mea}$ and $\left(\frac{C_t}{C_o}\right)_{pre}$ are the measured and predicted data, respectively. $\left(\frac{\overline{C_t}}{C_o}\right)_{mea}$ and $\left(\frac{\overline{C_t}}{C_o}\right)_{pre}$ are the average of $\left(\frac{C_t}{C_o}\right)_{mea}$ and $\left(\frac{C_t}{C_o}\right)_{pre}$, respectively, and n is the total number of data points. E_f and R^2 values close to 100 and 1, respectively, indicate that the accuracy of the model is higher. The prediction of the hybrid model is considered to be excellent, good, fair and poor, when $0 < NRMSE < 10$, $10\% < NRMSE < 20\%$, $20\% < NRMSE < 30\%$ and $NRMSE > 30\%$, respectively. The linear regression was also fitted for $\left(\frac{C_t}{C_o}\right)_{mea}$ and $\left(\frac{C_t}{C_o}\right)_{pre}$ as follows:

$$\left(\frac{C_t}{C_o}\right)_{mea} = m\left(\frac{C_t}{C_o}\right)_{pre} + n \tag{9}$$

where m and n are the regression coefficients.

Thomas model

The Thomas equation in linearized form is as follows (Thomas 1944):

$$\ln\left(\frac{C_o}{C_t} - 1\right) = \frac{k_{Th}q_{ads}m}{Q} - k_{Th}C_o t \tag{10}$$

where C_o (mg L^{-1}) and C_t (mg L^{-1}) are the influent Cd(II) concentration and effluent Cd(II) concentration at time t, respectively, m is the mass of the adsorbent (g), Q is the volumetric flow rate (mL min^{-1}), k_{Th} (mL min^{-1} mg^{-1}) is the Thomas rate constant and q_{ads} (mg g^{-1}) is the equilibrium Cd(II) uptake per g of the stabilized nZVI.

Sensitivity analysis for the hybrid model

Identification of the most important parameters for modeling BTCs is one of the key goals of this research. In this regard, the sensitivity analysis can provide important information regarding the modeling. As such, the influence index was calculated for each parameter as follows (Gontarski *et al.* 2000):

$$\text{Influence index} = II = 100\left(1 - \frac{R_i}{R_{CB}}\right) \tag{11}$$

where R_i is the correlation index between $\left(\frac{C_t}{C_o}\right)_{mea}$ and $\left(\frac{C_t}{C_o}\right)_{pre}$ for the hybrid model when one input factor is eliminated and R_{CB} is the correlation index between $\left(\frac{C_t}{C_o}\right)_{mea}$ and $\left(\frac{C_t}{C_o}\right)_{pre}$ for the hybrid model.

RESULTS AND DISCUSSION

A hybrid model (Thomas equation + ANFIS model)

The values of q_{ads} and k_{Th} in the Thomas equation can be determined using the linear regression approach, which may give unreliable results for unsymmetrical BTCs. As such, a new hybrid Thomas–ANFIS model has been developed for the dynamic adsorption of Cd(II) ions by ostrich bone
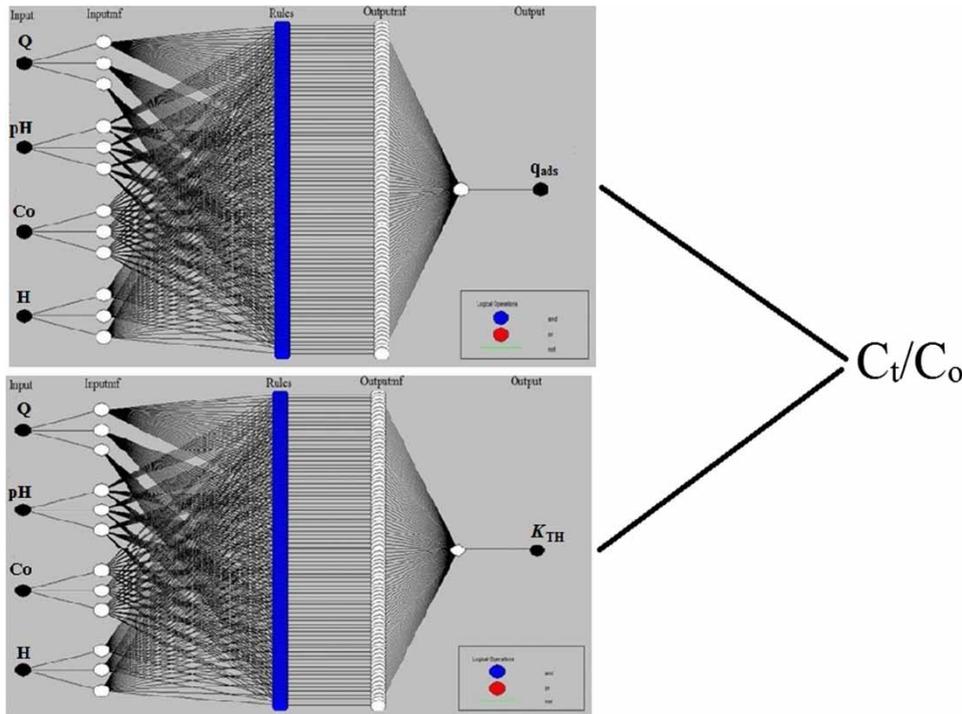
Figure 1 │ ANFIS architecture applied for predicting the $\frac{C_t}{C_o}$ using ostrich bone ash supported-nZVI composite.

ash-supported nZVI (see Figure 1). The Thomas–ANFIS model combines the best characteristics of the Thomas equation and ANFIS model in linear and non-linear prediction for data fitting of Cd(II). It is clear that some of the input variables have more statistical influence than others for the modeling of BTC. Thus, it is notable that only the substantial parameters are employed as inputs to the hybrid model. To select an appropriate ANFIS architecture, several configurations of input variables were analyzed using a trial and error procedure. Thus, one structure was evaluated for four input variables, four structures for three input variables, six structures for two input variables, and four structures for one input variables. The ANFIS structure with the highest E_f and smallest *NRMSE* was nominated as the best (Table S1, available with the online version of this paper), with four separate ANFIS models being found. The E_f, *NRMSE* and R^2 statistics for each ANFIS structure used to model the Cd(II) adsorption BTC in the testing period are presented in Table 1. It is obvious that the inclusion of all input variables in the ANFIS structure improves the accuracy of the Thomas parameters predicted. ANFIS4, the input variables for which are pH, Q, H and C_o, displays the best performance

($E_f = 93.8\%$, $R^2 = 0.996$, $NRMSE = 3.81\%$), followed by ANFIS3 ($E_f = 84.28\%$, $R^2 = 0.923$, $NRMSE = 13.49\%$), ANFIS2 ($E_f = 52.18\%$, $R^2 = 0.7289$, $NRMSE = 28.36\%$) and ANFIS1 ($E_f = 38.46\%$, $R^2 = 0.6463$, $NRMSE = 47.26\%$). Use of pH alone as the input variable gave the poorest q_{ads} and k_{Th} values. The poor performance of the hybrid model improved to fair upon increasing the input variables from pH alone to $pH + Q$. Similarly, a good performance of the hybrid model was achieved with pH, Q and H as the input variables. Finally, a hybrid architecture with pH, Q, H and C_o as inputs exhibited an excellent performance as regards predicting the Cd(II) adsorption BTC. The training process of the hybrid model for ANFIS4, ANFIS3, Structure1, Structure2 and Structure3 with time can be seen in Figure S7 (available online), which shows that NRMSE decreased with increasing number of epochs, remaining constant after 250. Clearly, the NRMSE calculates the differences between the estimated $\frac{C_t}{C_o}$ by hybrid model and the measured $\frac{C_t}{C_o}$ in the training dataset. Consequently, 250 epochs were adequate to train the hybrid model because value of error was fixed after this point, although the number of epochs depends on the problem
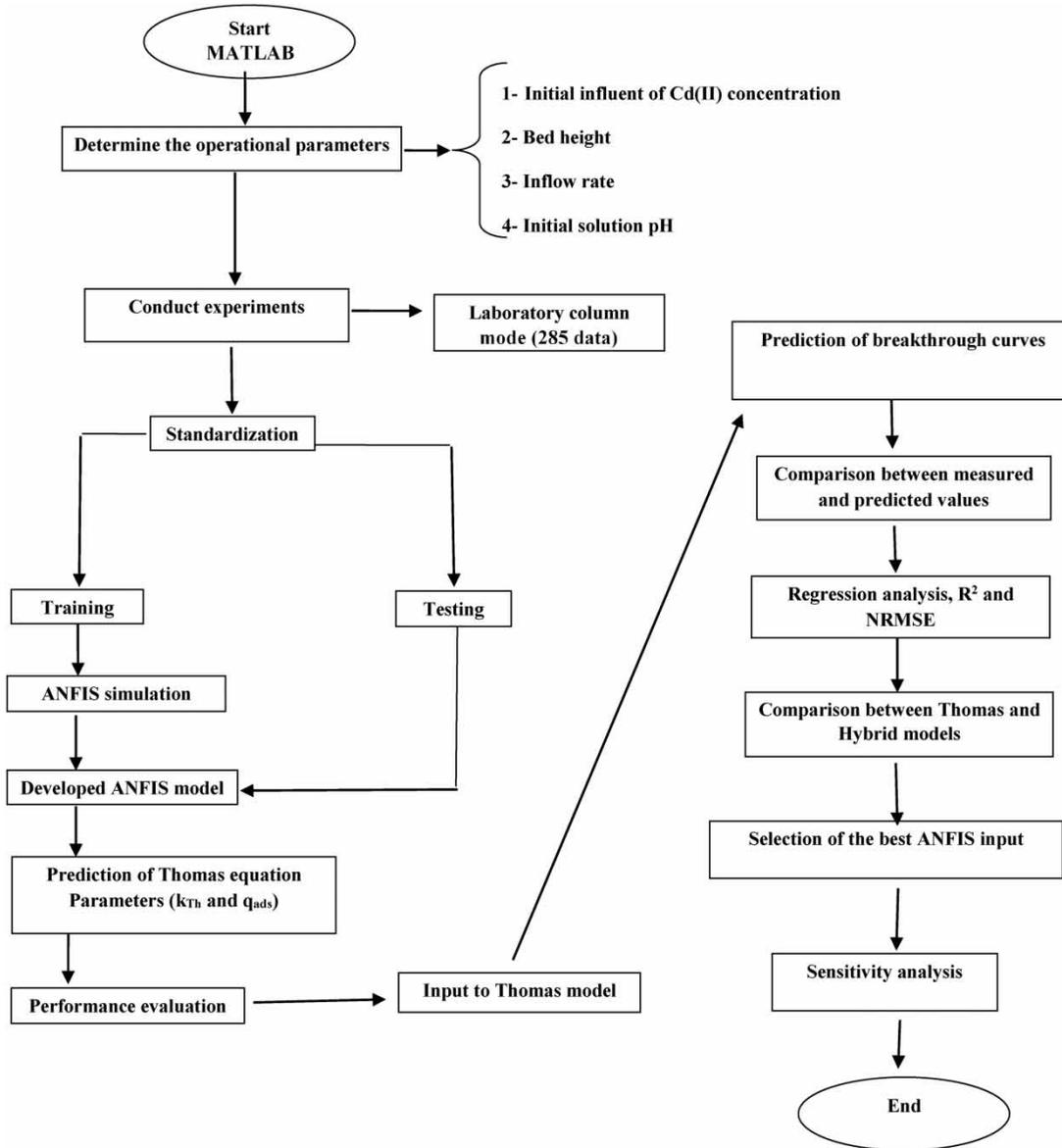
Figure 2 | Flowchart of computations in ANFIS–Thomas model.

Table 1 | Statistical performance evaluation criteria for the final models

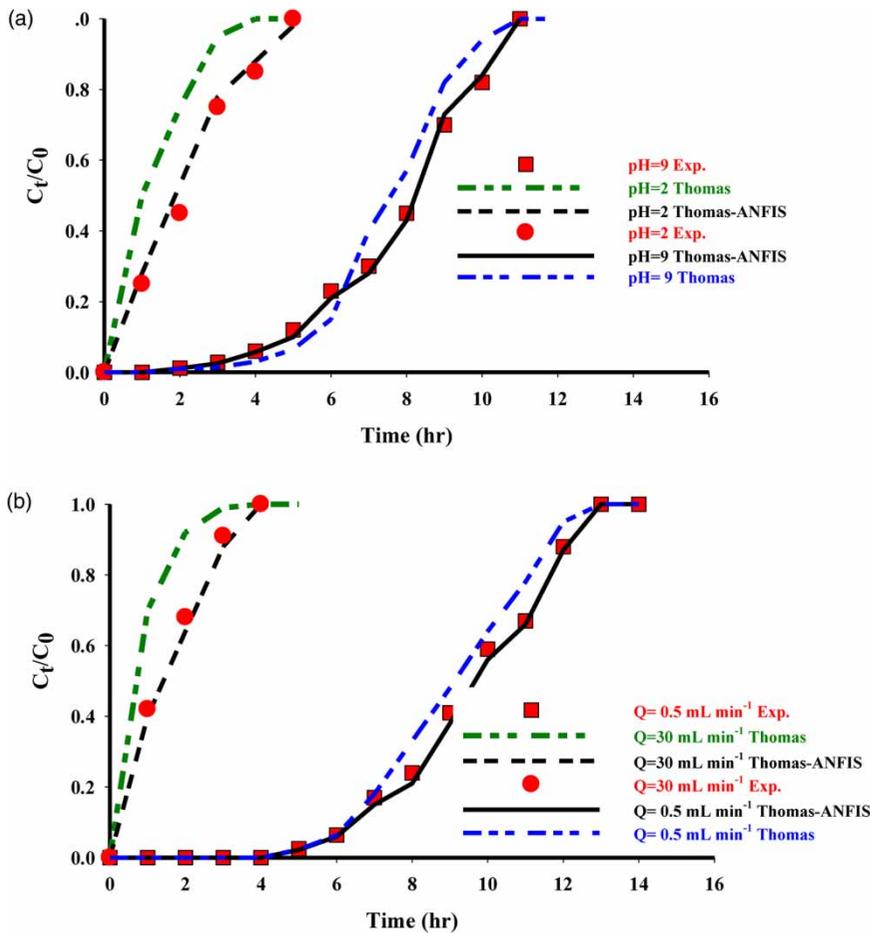| Model	Input	E_f	R^2	NRMSE	Performance	Rank
ANFIS4	pH, Q, H, C_o	93.8	0.9959	3.81	Excellent	1
ANFIS3	pH, Q, H	84.28	0.9231	13.49	Good	2
Structure3	pH, Q, C_o	71.66	0.8153	20.8	Fair	3
Structure2	pH, H, C_o	67.93	0.7461	22.34	Fair	4
Structure1	C_o, Q, H	44.87	0.6819	34.43	Poor	6
ANFIS2	pH, Q	52.18	0.7289	28.36	Fair	5
ANFIS1	pH	38.46	0.6463	47.26	Poor	7

Figure 3 │ Measured and predicted BTC of Cd(II) ions acquired by Thomas and hybrid models: (a) temperature, 25 ± 1 °C; influent concentration, 100 mg L^{-1}; bed height, 12 cm; influent flow rate, 1.5 mL min^{-1}; (b) temperature, 25 ± 1 °C; influent concentration, 100 mg L^{-1}; bed height, 12 cm; pH, 7.

(30 epochs by Singh *et al.* (2012); 100 epochs by Ho & Tsai (2011); 1,000 epochs by Amiri *et al.* (2013)). Using a small number of epochs causes poor learning and leads to underfitting, whereas a high number of epochs takes a long time to converge and leads to overfitting (Kisi & Ozturk 2007; Singh *et al.* 2012). However, the performance of all structures was excellent because the NRMSE values of them were lower than 10% in training phase.

Dynamic adsorption of Cd(II) under operating factors

Column experiments were performed under different key operating conditions varying the pH (see Figure 3(a)), *Q* (see Figure 3(b)), *H* (see Figure 4(a)), and *C*$_o$ (see Figure 4(b)). The pH of the solution is a key factor affecting the adsorption process due to ionization of the functional

groups in the structure of the adsorbent. In this experiment, the pH was changed from 2 to 9, while maintaining the other key operating conditions constant. This increase in pH increased the adsorption capacity, thus extending the BTC. The $\frac{C_t}{C_o}$ values were 0.06 and 0.85 at a pH of 9 and 2, respectively, in the interval of 4 h (see Figure 3(a)). Consequently, the removal efficiency of Cd(II) by ostrich bone ash-supported nZVI increases upon increasing the pH from 2 to 9. This could be due to the point of zero charge (pH$_{PZC}$) and the degree of ionization of Cd(II) (Amiri *et al.* 2016). The pH$_{PZC}$ of the adsorbent was about 5.87 and the pH at the ostrich bone ash-supported nZVI surface is neutral. However, the surface charge of the adsorbent is positive at a pH below 5.87 and is negative at any pH above 5.87 (Gil *et al.* 2018). The lowest Cd(II) uptake was
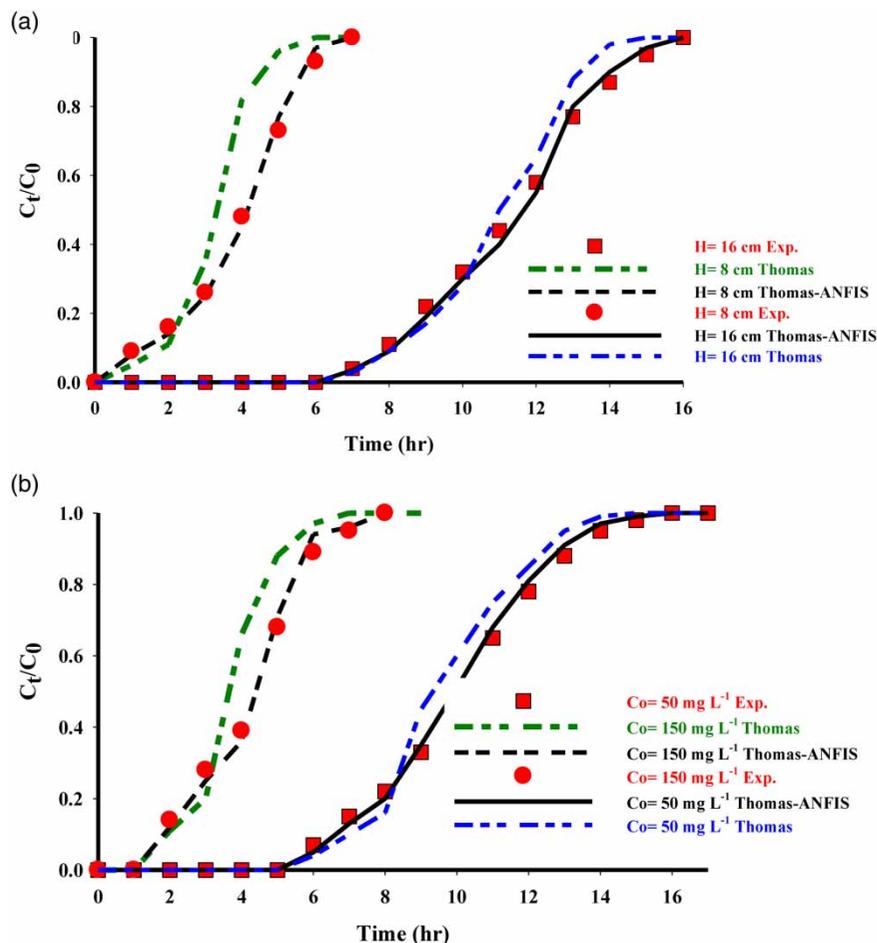
Figure 4 │ Measured and predicted BTC of Cd(II) ions acquired by Thomas and hybrid models: (a) temperature, $25 \pm 1\,°C$; influent concentration, $100\,mg\,L^{-1}$; influent flow rate, $1.5\,mL\,min^{-1}$; pH, 7; (b) temperature, $25 \pm 1\,°C$; bed height, 12 cm; influent flow rate, $1.5\,mL\,min^{-1}$; pH, 7.

observed at pH 2 as a result of competition between hydrogen ions and Cd^{2+} for binding sites on the adsorbent. In addition, a higher electrostatic repulsion between the Cd(II) ions and sorbent surface is observed at pH < 5.87. At pH > 5.87, increased deprotonation of the ostrich bone ash-supported nZVI surface causes a significant increase in the negatively charged sites, thus resulting in a higher electrostatic attraction between the adsorbent surface and Cd(II) ions (Soleymanzadeh *et al.* 2015; Amiri *et al.* 2016). Moreover, the higher removal efficiency of Cd(II) ions at pH 9 may be due to the precipitation of cadmium(II) as $Cd(OH)_2$.

Another key factor for dynamic Cd(II) adsorption in a fixed-bed column is related to the influent flow rate. As such, the BTC at six different Q (0.5, 1, 1.5, 10, 20 and $30\,mL\,min^{-1}$) was examined, while maintaining the C_o, H

and *pH*. An increase in Q from 0.5 to $30\,mL\,min^{-1}$ shifted the BT time and t_e to lower values, thus resulting in a lower adsorption capacity (Chowdhury & Saha 2013; Oguz 2017). The removal efficiency of Cd(II) by ostrich bone ash-supported nZVI increased in the order $Q = 30 < Q = 20 < Q = 10 < Q = 1.5 < Q = 1 < Q = 0.5\,mL\,min^{-1}$. The increase in Cd(II) removal as the Q decreased can be related to the longer mass transfer time for the sorption of Cd(II) by the binding sites (Cavas *et al.* 2011). Furthermore, a decrease in external film mass resistance on the ostrich bone ash-supported surface was observed at higher Q (Cavas *et al.* 2011). Thus, $\frac{C_t}{C_o}$ values of 0 and 1 were observed for Q of 0.5 and $30\,mL\,min^{-1}$, respectively, obtained in the interval of 4 h (see Figure 3(b)).

Given that the mass of adsorbent particles accumulated in the column and the pressure drop are more significant (Oguz 2017), the different adsorbent H studied ranged from 8 to 16 cm. The slope of the BTC decreased with rising H, thus resulting in a widened mass transfer zone. At $H = 8$ cm, an axial dispersion phenomenon is predominant, which results in a decrease in the diffusion of Cd(II) ions from solution into the pores of the adsorbent. The removal efficiency of Cd(II) ions by ostrich bone ash-supported nZVI was also found to increase upon increasing the H from 8 to 16 cm. This is due to the fact that the increase in H in the column probably increases the surface area, thus providing more binding sites for adsorption (Oguz & Ersoy 2014). The $\frac{C_t}{C_o}$ values were 0 and 0.48 for H of 16 and 8 cm, respectively, in the interval of 4 h (see Figure 4(a)).

The column BTC performance of ostrich bone ash-supported nZVI was studied using different C_o ranging from 50 to 150 mg L^{-1} (see Figure 4(b)), with t_e and BT time decreasing as the C_o increased. This is due to the fact that the mass transfer of Cd(II) ions from solution into the pores of the ostrich bone ash-supported nZVI occurs more rapidly at higher C_o. It was also found that the removal efficiency of Cd(II) by ostrich bone ash-supported nZVI increased in the order of $C_o = 150 < C_o = 100 < C_o = 50$ mg L^{-1}. The $\frac{C_t}{C_o}$ values were 0 and 0.39 for C_o of 50 and 150 mg L^{-1}, respectively, in the interval of 4 h (see Figure 4(b)). This phenomenon can be explained by the faster saturation of the adsorbent active sites at higher C_o, which results in a decrease in BT time (Oguz & Ersoy 2014; Oguz 2017).

Comparison between the Thomas and hybrid models

The BTCs acquired upon dynamic adsorption of Cd(II) ions by ostrich bone ash-supported nZVI were predicted using the Thomas and hybrid models (see Figures 3(a), 3(b), 4(a) and 4(b)). To assess the goodness of fit, NRMSE, E_f, linear regression and R^2 were calculated using measured and estimated data (see Table 2). As can be seen from Figures 3(a) to 4(b), the Thomas model can describe the experimental data for symmetrical BTCs under various operational parameters ($pH = 9$ in Figure 3(a); $Q = 0.5$ mL min^{-1} in Figure 3(b); $H = 16$ cm in Figure 4(a); $C_o = 50$ mg L^{-1} in Figure 4(b)). However, the performance of this model worsens for unsymmetrical BTCs ($pH = 2$ in Figure 3(a); $Q = 30$ mL min^{-1} in Figure 3(b); $H = 8$ cm in Figure 4(a); $C_o = 150$ mg L^{-1} in Figure 4(b)) and the difference between the experimental data and data estimated using the model increases. As can be seen from Figures 3(a) to 4(b), the new hybrid model is able to predict both the symmetric and asymmetric experimental BTCs under various key operating conditions. Indeed, higher R^2 and E_f values and smaller values of NRMSE are obtained when using the hybrid model compared to the Thomas model, thus indicating the higher accuracy of the hybrid model (see Table 2). Indeed, the fair performance of the Thomas model ($NRMSE = 27.6\%$ and $E_f = 64.6\%$) improved to excellent ($NRMSE = 3.8\%$ and $E_f = 93.8\%$) when combining this model with the ANFIS model to take advantage of the latter's unique advantages for nonlinear modeling. These findings are in a good agreement with those of Han *et al.* (2007), who reported that a nonlinear method is more effective than a linear method for predicting the parameters of the Thomas model. A comparison of the BTC estimated using the hybrid model and experimental data is depicted in Figure 5. The 95% prediction intervals, based on the distribution of points around the fitted line, exhibit an excellent reliability for the fitting and prediction of BTCs (see Figure 5). The error histogram of the BTC for the hybrid model is presented in Figure 6. As can be seen, the error

Table 2 | The performance of Thomas and Thomas–ANFIS models to predict BTC

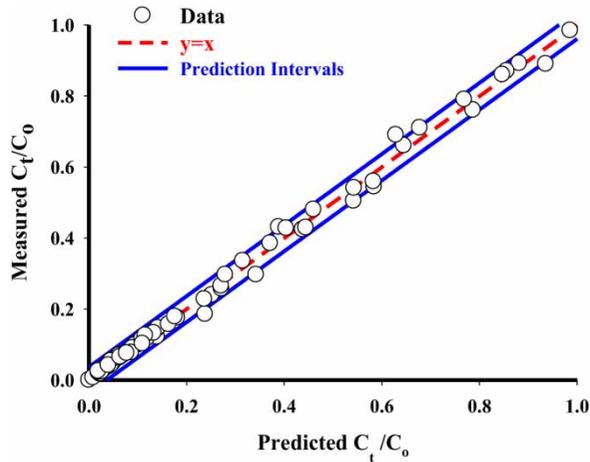| Model	Equation	E$_f$ (%)	R^2	NRMSE (%)	Performance
Thomas–ANFIS	$\left(\dfrac{C_t}{C_o}\right)_{mea} = 1.002\left(\dfrac{C_t}{C_o}\right)_{pre} + 0.0014$	93.8	0.9959	3.8	Excellent
Thomas	$\left(\dfrac{C_t}{C_o}\right)_{mea} = 1.12\left(\dfrac{C_t}{C_o}\right)_{pre} + 3.65$	64.6	0.8443	27.6	Fair

Figure 5 | Comparison of the BTC predicted by hybrid model and experimental data.

distribution is very close to zero and is almost symmetrically bell-shaped, thus indicating that hybrid model satisfies the suppositions of normality. As such, this hybrid model can be a fast and accurate alternative to the mathematical empirical equations currently available.

Sensitivity analysis

The sensitivity of the hybrid model to input variables is presented in Table 3. The changes in influence index (%) upon elimination of each input parameter from the hybrid model are presented in Table 3. It is obvious that initial solution pH is the most sensitive parameter, followed by Q, H and C_o. All
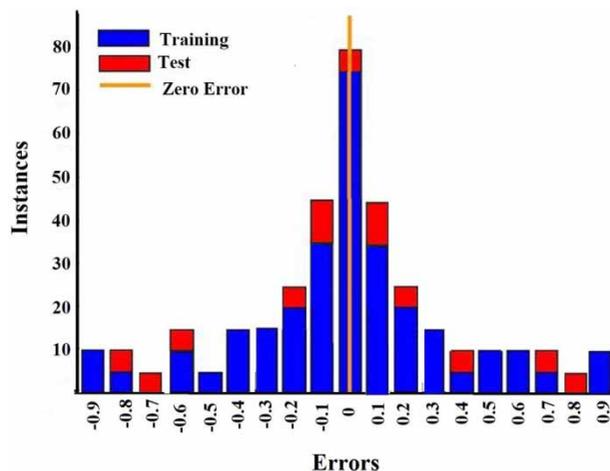

Figure 6 | Error histogram of the hybrid model.

Table 3 | The sensitivity of hybrid model to each input variable

Model	Input	Eliminated parameter	Influence index (%)
Hybrid model	pH, Q, H, C_o	–	–
Structure1	Q, H, C_o	pH	17.082
Structure2	pH, H, C_o	Q	13.26
Structure3	pH, Q, C_o	H	9.33
ANFIS3	pH, Q, H	C_o	3.52

four operating parameters in Table 3 are considered to be important for the hybrid model as the lowest value of the influence index was significant. Thus, Table 3 shows that an increase in pH, Q, H and C_o is significant at 17.082, 13.26, 9.33 and 3.52, respectively.

Calculation of k_{Th} and q_{ads} using the Thomas and hybrid models

The q_{ads} values for Cd(II) dynamic adsorption using experimental data are compared with those calculated using the Thomas and hybrid models in Table 4. The q_{ads} calculated using the linear regression of the Thomas model is acceptable at the greatest H and lowest Q and C_o (see Table 4). However, the linear regression of the Thomas model, which is the most widely used approach for modeling BTCs, provides a poor estimate of q_{ads} at higher Q and C_o (see Table 4). Thus, although the Thomas model is suitable for data modeling in the case of symmetrical BTCs, it may fail to correctly describe the performance of unsymmetrical BTCs. However, the hybrid model is able to predict both symmetrical and asymmetrical experimental BTCs. For instance, the q_{ads} values obtained using experimental data, and the Thomas and hybrid models were found to be 5.24, 5.39 and 5.31 mg g^{-1}, respectively, at $pH = 7$; $Q = 1$ mL min^{-1}; $H = 16$ cm and $C_o = 50$ mg L^{-1}. Similarly, q_{ads} values of 3.03, 4.02 and 2.98 mg g^{-1} were obtained using experimental data, and the Thomas and hybrid models, respectively, at $pH = 7$; $Q = 10$ mL min^{-1}; $H = 8$ cm and $C_o = 150$ mg L^{-1}. Similar results have been observed for k_{Th} with values ranging from 0.24 to 1.56 mL min^{-1} mg^{-1} for the Thomas model and 0.21–1.42 mL min^{-1} mg^{-1} for the hybrid model. Clearly, the obtained values of q_{ads} and k_{Th} by Thomas and hybrid models vary dramatically under

Table 4 | Calculated design parameters using Thomas and hybrid models for dynamic adsorption of Cd(II) ions by OBA/nZVI

| | | | Results of design parameter | | | | |
| | | | q_{ads} (mg g^{-1}) | | | k_{Th} (mL min^{-1} mg^{-1}) | |
Flow rate (mL min^{-1})	Bed depth (cm)	Cd(II) concentration (mg L^{-1})	Experimental	Thomas model	Hybrid model	Thomas model	Hybrid model
1	8	50	4.64	4.86	4.69	0.72	0.68
1	8	150	3.52	3.81	3.47	1.19	1.08
10	8	50	4.04	4.62	3.98	1.05	0.79
10	8	150	3.03	4.02	2.98	1.56	1.42
1	16	50	5.24	5.39	5.31	0.24	0.21
1	16	150	3.96	4.18	3.85	0.47	0.42
10	16	50	4.52	4.94	4.41	0.43	0.36
10	16	150	3.32	4.34	3.41	0.61	0.54

experimental conditions (see Table 4). In addition, the relative differences between the calculated q_{ads} of hybrid model were smaller than those in the Thomas model for each operating condition. As a result, the hybrid model provides the flexibility of reliably estimating the performance of fixed bed column at various operational conditions. Similar results were reported by Tovar-Gomez *et al.* (2013). Furthermore, the estimated k_{Th} by Thomas and hybrid models increased with increasing the influent Cd(II) concentration and inlet flow rates demonstrating that the driving force of Cd(II) mass transfer is also raised. Similar trends were also observed by Cavas *et al.* (2011) for adsorption of methylene blue by a beach waste dead leaves.

CONCLUSIONS

The present study reveals a novel hybrid model that combines both Thomas and ANFIS models, to predict BTCs for Cd(II) ions in a fixed-bed column. The dynamic adsorption of Cd(II) ions on ostrich bone ash-supported nZVI was studied as a function of initial solution pH, influent flow rate, bed height and initial Cd(II) concentration. The results indicate the following:

1. The fair performance of the Thomas model ($NRMSE = 27.6\%$ and $E_f = 64.6\%$) improves to excellent ($NRMSE = 3.8\%$ and $E_f = 93.8\%$) when combining this model with ANFIS.

2. The hybrid model provides more reliable results as regards predicting the performance of BTC compared to the Thomas model.

3. The sensitivity analysis indicates that initial solution pH is a more significant input variable for the hybrid model than the other operational factors.

4. This hybrid model can be employed for data modeling of any unsymmetrical BTC or natural surface and groundwater, as it provides a powerful tool for accurate nonlinear modeling and is also capable of learning from the environment.

5. The suggested adsorbent is a versatile and eco-friendly material for attenuating cadmium ions in a fixed-bed column.

REFERENCES

Amiri, M. J. & Shabani, A. 2017 Application of adaptive neural-based fuzzy inference system model for predicting leaf area. *Comm. Soil Sci. Plant Anal.* **48** (14), 1669–1683.

Amiri, M. J., Abedi-Koupai, J., Eslamian, S. S., Mousavi, S. F. & Hasheminejad, H. 2013 Modeling Pb(II) adsorption from aqueous solution by ostrich bone ash using adaptive neural-based fuzzy inference system. *J. Environ. Sci. Health A* **48** (5), 543–558.

Amiri, M. J., Abedi-Koupai, J., Eslamian, S. S. & Arshadi, M. 2016 Adsorption of Pb(II) and Hg(II) ions from aqueous single metal solutions by using surfactant-modified ostrich bone waste. *Desal. Water Treat.* **57**, 16522–16539.

Amiri, M. J., Abedi-Koupai, J. & Eslamian, S. 2017 Adsorption of Hg(II) and Pb(II) ions by nanoscale zero-valent iron

supported on ostrich bone ash in a fixed-bed column system. *Water Sci. Technol.* **76**, 671–682.

Arshadi, M., Gholtash, J. E., Zandi, H. & Foroughifard, S. 2015 Phosphate removal by a nano-biosorbent from the synthetic and real (Persian Gulf) water samples. *RSC Adv.* **5** (54), 43290–43302.

Bohart, G. & Adams, E. Q. 1920 Some aspects of the behavior of charcoal with respect to chlorine. *J. Am. Chem. Soc.* **42**, 523–544.

Boparai, H. K., Joseph, M. & O'Carroll, D. M. 2011 Kinetics and thermodynamics of cadmium ion removal by adsorption onto nanozerovalent iron particles. *J. Hazard. Mater.* **186**, 458–465.

Boparai, H. K., Joseph, M. & O'Carroll, D. M. 2013 Cadmium (Cd^{2+}) removal by nano zerovalent iron: surface analysis, effects of solution chemistry and surface complexation modeling. *Environ. Sci. Pollut. Res.* **20**, 6210–6221.

Cavas, L., Karabay, Z., Alyuruk, H., Dogan, H. & Demir, G. K. 2011 Thomas and artificial neural network models for the fixed-bed adsorption of methylene blue by a beach waste *Posidonia oceanica* (L.) dead leaves. *Chem. Eng. J.* **171** (2), 557–562.

Chowdhury, S. & Saha, P. 2013 Artificial neural network (ANN) modeling of adsorption of methylene blue by NaOH-modified rice husk in a fixed-bed column system. *Environ. Sci. Pollut. Res.* **20** (2), 1050–1058.

Gil, A., Amiri, M. J., Abedi-Koupai, J. & Eslamian, S. 2018 Adsorption/reduction of Hg (II) and Pb (II) from aqueous solutions by using bone ash/nZVI composite: effects of aging time, Fe loading quantity and co-existing ions. *Environ. Sci. Pollut. Res.* **25** (3), 2814–2829.

Gontarski, C. A., Rodrigues, P. R., Mori, M. & Prenem, L. F. 2000 Simulation of an industrial wastewater treatment plant using artificial neural networks. *Comput. Chem. Eng.* **24**, 1719–1723.

Han, R., Wang, Y., Zou, W., Wang, Y. & Shi, J. 2007 Comparison of linear and nonlinear analysis in estimating the Thomas model parameters for methylene blue adsorption onto natural zeolite in fixed-bed column. *J. Hazard. Mater.* **145**, 331–335.

Hasan, S. H., Ranjan, D. & Talat, M. 2010 Agro-industrial waste 'wheat bran' for the biosorptive remediation of selenium through continuous up-flow fixed-bed column. *J. Hazard. Mater.* **181**, 1134–1142.

Ho, Y. & Tsai, C. 2011 Comparing ANFIS and SEM in linear and nonlinear forecasting of new product development performance. *Expert Syst. Appl.* **38**, 6498–6507.

Hutchins, R. A. 1973 New method simplifies design of activated carbon systems, water bed depth service time analysis. *Chem. Eng.* **80**, 133–138.

Kisi, O. & Ozturk, O. 2007 Adaptive neurofuzzy computing technique for evapotranspiration estimation. *J. Irrig. Drain. Eng. ASCE* **4** (133), 368–379.

Masomi, M., Ghoreyshi, A. A., Najafpour, G. D. & Mohamed, A. R. B. 2015 Dynamic adsorption of phenolic compounds on activated carbon produced from pulp and paper mill sludge: experimental study and modeling by artificial neural network (ANN). *Desal. Water Treat.* **55** (6), 1453–1466.

Mousavi, S. F. & Amiri, M. J. 2012 Modeling nitrate concentration of groundwater using adaptive neural-based fuzzy inference system. *Soil Water Res.* **7** (2), 73–83.

Oguz, E. 2017 Fixed-bed column studies on the removal of Fe^3 and neural network modelling. *Arab. J. Chem.* **10** (3), 313–320.

Oguz, E. & Ersoy, M. 2014 Biosorption of cobalt(II) with sunflower biomass from aqueous solutions in a fixed bed column and neural networks modelling. *Ecotoxicol. Environ. Saf.* **99**, 54–60.

Singh, R., Kainthola, A. & Singh, T. N. 2012 Estimation of elastic constant of rocks using an ANFIS approach. *Appl. Soft Comput.* **12**, 40–45.

Soleymanzadeh, M., Arshadi, M., Salvacion, J. W. L. & SalimiVahid, F. 2015 A new and effective nanobiocomposite for sequestration of Cd (II) ions: nanoscale zerovalent iron supported on sineguelas seed waste. *Chem. Eng. Res. Des.* **93**, 696–709.

The Council of the European Communities 1976 Directive on pollution caused by certain dangerous substances discharged into the aquatic environment of the community [76/464/EEC]. *Off. J. Eur. Commun. L* 129/23 (May).

Thomas, H. C. 1944 Heterogeneous ion exchange in a flowing system. *J. Am. Chem. Soc.* **66**, 1664–1666.

Tovar-Gomez, R., Moreno-Virgen, M. R., Dena-Aguilar, J. A., Hernandez-Montoya, V., Bonilla-Petriciolet, A. & Montes-Moran, M. A. 2013 Modeling of fixed-bed adsorption of fluoride on bone char using a hybrid neural network approach. *Chem. Eng. J.* **228**, 1098–1109.

Yoon, Y. H. & Nelson, J. H. N. 1984 Application of gas adsorption kinetics. *Am. Ind. Hyg. Assoc. J.* **45**, 509–516.

Zhang, X., Lin, S., Chen, Z., Megharaj, M. & Naidu, R. 2011 Kaolinite-supported nanoscale zero-valent iron for removal of Pb^{2+} from aqueous solution: reactivity, characterization and mechanism. *Water Res.* **45**, 3481–3488.

Zhang, Y., Li, Y., Dai, C., Zhou, X. & Zhang, W. 2014 Sequestration of Cd(II) with nanoscale zero-valent iron (nZVI): characterization and test in a two-stage system. *Chem. Eng. J.* **244**, 218–226.